

# Theoretical description of phase coexistence in model $C_{60}$

D. Costa\*, G. Pellicane, and C. Caccamo

*Istituto Nazionale per la Fisica della Materia (INFN) and Dipartimento di Fisica  
Università di Messina, Contrada Papardo, C.P. 50, 98166 Messina – Italy*

E. Schöll-Paschinger and G. Kahl

*Institut für Theoretische Physik and CMS, TU Wien  
Wiedner Hauptstraße 8-10, A-1040 Wien – Austria*

We have investigated the phase diagram of a pair interaction model of  $C_{60}$  fullerene [L. A. Girifalco, J. Phys. Chem. **96**, 858 (1992)], in the framework provided by two integral equation theories of the liquid state, namely the Modified Hypernetted Chain (MHNC) implemented under a global thermodynamic consistency constraint, and the Self-Consistent Ornstein-Zernike Approximation (SCOZA), and by a Perturbation Theory (PT) with various degrees of refinement, for the free energy of the solid phase.

We present an extended assessment of such theories as set against a recent Monte Carlo study of the same model [D. Costa, G. Pellicane, C. Caccamo, and M. C. Abramo, J. Chem. Phys. **118**, 304 (2003)]. We have compared the theoretical predictions with the corresponding simulation results for several thermodynamic properties like the free energy, the pressure, and the internal energy. Then we have determined the phase diagram of the model, by using either the SCOZA, or the MHNC, or the PT predictions for one of the coexisting phases, and the simulation data for the other phase, in order to separately ascertain the accuracy of each theory. It turns out that the overall appearance of the phase portrait is reproduced fairly well by all theories, with remarkable accuracy as for the melting line and the solid-vapor equilibrium. All theories show a more or less pronounced discrepancy with the simulated fluid-solid coexistence pressure, above the triple point. The MHNC and SCOZA results for the liquid-vapor coexistence, as well as for the corresponding critical points, are quite accurate; the SCOZA tends to underestimate the density corresponding to the freezing line. All results are discussed in terms of the basic assumptions underlying each theory.

We have selected the MHNC for the fluid and the first-order PT for the solid phase, as the most accurate tools to investigate the phase behavior of the model in terms of purely theoretical approaches. It emerges that the use of different procedures to characterize the fluid and the solid phases provides a semiquantitative reproduction of the thermodynamic properties of the  $C_{60}$  model at issue.

The overall results appear as a robust benchmark for further theoretical investigations on higher order  $C_{n>60}$  fullerenes, as well as on other fullerene-related materials, whose description can be based on a modelization similar to that adopted in this work.

PACS numbers: 61.20.Gy, 61.48.+c, 64.70.-p

## I. INTRODUCTION

A current model for  $C_{60}$  is based on a “smeared out” spherical representation of the fullerene molecules, early proposed by Girifalco [1], where the carbon atoms give rise to a uniform interaction distributed over the molecular cage surface. A straightforward integration leads to an analytical central pair potential, characterized by a harsh repulsive core followed by a deep attractive well, which rapidly decays with the interparticle distance.

A detailed characterization of the thermodynamic properties of the Girifalco model is of relevant interest in several respects: for instance, first-principle studies of the  $C_{60}$  interaction give results very similar to those predicted through the Girifalco model [2, 3]; the latter has been widely used to model  $C_{n>60}$  fullerenes with  $n = 70$ ,

76, and 84 (see [4, 5, 6, 7] and references cited therein), as well as other hollow nanoparticles like carbon onions and metal dichalcogenides like GaAs and CdSe (also termed inorganic fullerenes) [8]. Umiguchi and coworkers [9] proposed a semiempirical modification of the Girifalco interaction to account for the behavior of solid  $C_{60}$  at low temperature; such a generalization might prove useful for the analysis of the lattice properties under impurity doping.

As far as a more speculative analysis of the Girifalco model is concerned, several intriguing aspects are related to the overall appearance of its phase portrait, characterized by a narrow liquid pocket that extends only a few tens degrees over the triple point temperature [10, 11]. This borderline behavior, as for the existence of a stable liquid phase, basically depends on the interplay between entropic demands, imposed by excluded-volume effects at short distance, and energetic contributions, due to the attractive part of the interaction potential. We may recall, as an indication of the implied subtleties, the early controversy on the location of the liquid-vapor critical

---

\*Corresponding author, e-mail: [costa@tritone.unime.it](mailto:costa@tritone.unime.it)

point [12, 13], clarified in successive studies [14, 15], and the discrepancies on the position of the freezing line and of the triple point, related to the procedure adopted for the calculation of the liquid-solid equilibrium [10, 13, 16]. Recently (and unexpectedly, on the basis of a previous study on the Lennard-Jones fluid [17]), Fartaria and coworkers [3] have found that even the same simulation approach leads to distinct predictions on the freezing line of the Girifalco model, provided that different starting thermodynamic conditions are employed.

We have recently reconciled such disparate results in the context of extensive Monte Carlo calculations of the free energies of both the fluid and the solid phases of the model [11, 18]. We have concluded that the solid-fluid equilibrium is strongly affected by the deep, short-range attractive well in the interaction potential, at variance with systems whose freezing behavior is essentially dominated by steric effects. As a consequence, the freezing transition of the fluid is driven to lower densities (and the liquid pocket is reduced accordingly), mainly by energetic effects, in agreement with a common scenario recently proposed for fluids interacting through short-range forces [19].

The unusual aspects of the phase behavior have occasioned several studies on the  $C_{60}$  model by means of refined theoretical tools, like for instance integral equation theories for the fluid phase [13, 16], various density functional approximations [14, 20, 21], and the hierarchical reference theory [22]. Preliminary studies have been recently carried out, based on the Modified Hypernetted Chain approach (MHNC, [23]), solved under a global thermodynamic consistency constraint [24], and on the Self-Consistent Ornstein-Zernike Approximation (SCOZA [25, 26, 27]) [28]. However, such investigations were often compared to simulation results later revised; for example, several authors [13, 16, 28] have estimated the freezing conditions on the basis of some well-known one-phase structural indicators, as the Hansen-Verlet [29], or the Giaquinta and Giunta [30] criteria, whose limited applicability in the context of “energetic” fluids has been discussed in [11].

Hinging on the simulation study of Ref. [11], it is now worth reconsidering a detailed analysis of theoretical predictions for the phase diagram of the envisaged model. Following our preliminary investigations [24, 28] we shall adopt the MHNC and SCOZA theories to characterize the thermodynamic properties of the fluid phase. As far as the free energy of the solid phase is concerned, we use a Perturbation Theory (PT), discussing several degrees of refinement, as fully described in the text. Recent studies (see [31, 32] and references) have demonstrated that the PT accurately describes the solid phase and the solid-fluid transition of models characterized by short-range interactions, as the depletion potentials resulting from the effective one-component representation of hard-sphere mixtures. A second-order expansion for the PT, also analyzed in this work, has been used in Ref. [33] to investigate the phase behavior of several simple models

for globular protein solutions.

This paper is organized as follows: the theoretical approaches are described in section II. Results are reported and discussed in Section III. A short overview of our results and the conclusions are drawn in Section IV.

## II. MODEL AND THEORETICAL APPROACHES

### A. The Girifalco model potential

The Girifalco potential is well known in the fullerene literature, so we recall only its analytical expression [1],

$$v(r) = -\alpha_1 \left[ \frac{1}{s(s-1)^3} + \frac{1}{s(s+1)^3} - \frac{2}{s^4} \right] + \alpha_2 \left[ \frac{1}{s(s-1)^9} + \frac{1}{s(s+1)^9} - \frac{2}{s^{10}} \right], \quad (1)$$

where  $s = r/d$ ,  $\alpha_1 = N^2 A/12d^6$ , and  $\alpha_2 = N^2 B/90d^{12}$ ;  $N$  and  $d$  are the number of carbon atoms and the diameter, respectively, of the fullerene particles,  $A = 32 \times 10^{-60}$  erg cm<sup>6</sup> and  $B = 55.77 \times 10^{-105}$  erg cm<sup>12</sup> are constants entering the Lennard-Jones 12-6 potential through which two carbon sites on different spherical molecules are assumed to interact [1]. For  $C_{60}$ ,  $d = 0.71$  nm while the node of the potential (1), the minimum, and its position, are  $r_0 \simeq 0.959$  nm,  $\varepsilon \simeq 0.444 \times 10^{-12}$  erg and  $r_{\min} = 1.005$  nm, respectively.

### B. Perturbation theory of the solid phase

The perturbation approach is based on a separation of the potential (1) into a reference (purely repulsive) part,  $v_{\text{ref}}(r)$ , and a residual, attractive part,  $v_{\text{pert}}(r)$ . The reference system is then approximated by a solid of hard spheres with the same crystallographic structure, by means of a suitable definition of the hard-core diameter. Given these positions, the free energy of the system can be expanded around the free energy of the hard-sphere crystal,  $F_{\text{hs}}$ , to obtain at first order [34]:

$$\frac{\beta F}{N} = \frac{\beta F_{\text{hs}}}{N} + \frac{\beta \rho}{2} \int v_{\text{pert}}(r) \bar{g}_{\text{hs}}(r) \, \text{d}r, \quad (2)$$

where  $N$  is the number of particles,  $\beta$  the inverse of the temperature  $T$  in units of the Boltzmann constant, and  $\rho$  the number density; the second term is the thermal average of the perturbation energy over the reference system, where  $\bar{g}_{\text{hs}}(r)$  is the angular average of the pair distribution function of the hard-sphere solid,  $\rho^{(2)}(\mathbf{r}_1, \mathbf{r}_2)$  [35, 36].

We have followed the WCA prescription (after Weeks, Chandler, and Andersen [37]) to split the potential (1),

namely:

$$\begin{aligned} v_{\text{ref}}(r) &= \begin{cases} v(r) + \varepsilon & \text{if } r \leq r_{\min} \\ 0 & \text{if } r > r_{\min} \end{cases} \\ v_{\text{pert}}(r) &= \begin{cases} -\varepsilon & \text{if } r \leq r_{\min} \\ v(r) & \text{if } r > r_{\min} \end{cases} \end{aligned} \quad (3)$$

The properties of the reference system have been connected to those of the hard-sphere solid through the “blip function” formalism [38], i.e. the effective hard-sphere diameter  $\sigma_{\text{WCA}}$  is determined by the implicit relation:

$$\int y_{\text{hs}}(r) \{ \exp[-\beta v_{\text{pert}}(r)] - \exp[-\beta v_{\text{hs}}(r)] \} \mathbf{dr} = 0, \quad (4)$$

where  $v_{\text{hs}}(r)$  is the hard-sphere potential (which depends on  $\sigma_{\text{WCA}}$ ) and  $y_{\text{hs}}(r) = g_{\text{hs}}(r) \exp[\beta v_{\text{hs}}(r)]$  is the corresponding cavity function. Another definition of the hard-core diameter (BH, [39]), namely:

$$\sigma_{\text{BH}} = \int_0^\infty \{ 1 - \exp[-\beta v_{\text{pert}}(r)] \} \mathbf{dr} \quad (5)$$

has been tested in this work. The expression (5), which corresponds to a first-order approximation to Eq. (4) [34], is appropriate to describe the rapidly rising repulsive interaction  $v_{\text{pert}}(r)$ . Other prescriptions for the separation of the potential (1) (see Refs. [39] and [40]) have been analyzed in this study; their predictions for the thermodynamic properties of the model at issue are, however, less accurate on the whole than those obtained through the WCA approach and will not be discussed further.

In the results’ section we also investigate a second-order correction to the free energy, early proposed by Barker and Henderson in Ref. [41], and recently applied to systems with short-range interactions by Foffi and coworkers [33], namely:

$$\begin{aligned} \frac{\beta F}{N} &= \frac{\beta F_{\text{hs}}}{N} + \frac{\beta \rho}{2} \int v_{\text{pert}}(r) \bar{g}_{\text{hs}}(r) \mathbf{dr} \\ &\quad - \frac{\beta \rho}{4} \left( \frac{\partial \rho}{\partial P_{\text{hs}}} \right) \int v_{\text{pert}}(r)^2 \bar{g}_{\text{hs}}(r) \mathbf{dr}, \end{aligned} \quad (6)$$

where  $P_{\text{hs}}$  is the pressure of the solid of hard spheres. The correction in Eq. (6) was obtained by dividing the space into concentric spherical shells, and assuming that the volume of each shell has the compressibility properties of a macroscopic portion of the space (see Ref. [41] for full details on the procedure and the approximations involved).

We have resorted to several well-established simulation results in order to obtain the properties of the hard-sphere crystal. Specifically, we have used the Hall analytical equation of state for the pressure [42], which accurately fits the molecular dynamics data of Alder and coworkers [43]:

$$\frac{\beta P_{\text{hs}}}{\rho} = \frac{3\eta}{\eta_{\text{cp}} - \eta} + \sum_{n=0}^6 a_n \gamma^n \quad (7)$$

where  $\eta$  is the packing fraction and  $\eta_{\text{cp}} = \pi\sqrt{2}/6$  is the close packing fraction;  $\gamma = 4(1 - \eta/\eta_{\text{cp}})$  and  $a_0 = 2.557696$ ,  $a_1 = 0.1253077$ ,  $a_2 = 0.1762393$ ,  $a_3 = -1.053308$ ,  $a_4 = 2.818621$ ,  $a_5 = -2.921934$ ,  $a_6 = 1.118413$ . The free energy is obtained by thermodynamic integration

$$\frac{\beta F_{\text{hs}}(\rho)}{N} = \frac{\beta F_{\text{hs}}(\bar{\rho})}{N} + \int_{\bar{\rho}}^{\rho} \frac{\beta P_{\text{hs}}(\rho')}{\rho'} \frac{d\rho'}{\rho'}, \quad (8)$$

where for the reference free energy,  $F_{\text{hs}}(\bar{\rho})$ , we have used the Frenkel and Ladd [44] Monte Carlo result for the FCC crystal of hard spheres, namely:  $\beta F_{\text{hs}}^{\text{ex}}/N = 6.5379(09)$  at  $\eta/\eta_{\text{cp}} = 0.7778$  in the thermodynamic limit. Their determination followed the Einstein crystal method, based on the construction of a reversible path from the solid under consideration to an Einstein crystal with the same crystallographic structure. As for the radial distribution function,  $\bar{g}_{\text{hs}}(r)$ , we have used the analytical form, proposed by Weis [35] and Kincaid and Weis [45], which expresses the distribution as a sum of gaussian peaks centered around the nearest-neighbour FCC lattice sites, with parameters calculated by Choi and coworkers [40] to fit their simulation results. In Ref. [40] an analytical form for the cavity function  $y_{\text{hs}}(r)$  inside the hard core entering Eq. (4) is also proposed, by directly extending to the solid the Henderson and Grundke scheme for the fluid phase [46].

### C. Liquid state theories

We have determined the thermodynamic and structural properties of the fluid region through the MHNC [23] and SCOZA [25] theories. We recall that in the MHNC the Ornstein-Zernike equation,

$$h(r) = c(r) + \rho \int c(|\mathbf{r} - \mathbf{r}'|) h(r') \mathbf{dr}', \quad (9)$$

is coupled with the cluster expansion for the radial distribution function  $g(r)$ , namely:

$$g(r) = \exp[-\beta v(r) + h(r) - c(r) + B(r)], \quad (10)$$

where  $h(r) = [g(r) - 1]$  and  $c(r)$  are the pair and direct correlation functions respectively, and  $B(r)$  is the bridge function [34]. A closure to Eqs. (9) and (10) is obtained through the Percus-Yevick hard-sphere bridge function  $B^{\text{PY}}(r, \sigma_{\text{hs}}^*)$ , with the hard-core diameter  $\sigma_{\text{hs}}^*$  fixed so to enforce the thermodynamic consistency of the theory (see e.g. [47]). In particular we require the equality between the fluctuation pressure  $P_c$  and the virial pressure  $P_v$ , namely,

$$P_c \equiv \beta^{-1} \int_0^\rho \frac{\chi_0}{\chi_T} d\rho' = P_v. \quad (11)$$

In Eq. (11)  $\chi_0$  and  $\chi_T$  are the ideal gas and the isothermal compressibilities respectively; the latter is obtained

as the  $q = 0$  limit of the Fourier transform of the direct correlation function,  $\chi_0/\chi_T = [1 - \rho\tilde{c}(q = 0)]$ , according to the fluctuation theory; the density integral is performed at a constant temperature.

The consistency between  $P_v$  and the pressure estimated via the energy route,  $P_e$ , can be alternatively enforced along isochoric paths, namely:

$$P_e \equiv \rho^2 \left. \frac{\partial F}{\partial \rho} \right|_T = P_v. \quad (12)$$

In Eq. (12) the free energy is obtained by integrating the internal energy  $U$  with respect to the (inverse) temperature at constant density, according to the relation:

$$\frac{\beta F(\rho, T)}{N} = \frac{\beta F(\rho, \bar{T})}{N} - \int_{\bar{T}}^T \frac{U(T')}{Nk_B T'} \frac{dT'}{T'}, \quad (13)$$

where  $(\rho, \bar{T})$  is a thermodynamic state whose absolute free energy  $\beta F(\rho, \bar{T})/N$  is known. In order to avoid to cross the liquid-vapor coexistence region, combinations of isothermal and isochoric paths are required to reach thermodynamic points located in the high-density, sub-critical region of the phase diagram.

As shown in Ref. [24], the global consistency is in general more accurate than the local one; the latter procedure enforces the equality between the isothermal compressibility calculated via the fluctuation theory on the one hand, and via the virial route (i.e. by differentiating  $P_v$  with respect to the density) on the other hand. The improvement of the global over the local consistency approach becomes crucial when the range of the particle interaction is very short, and/or at high densities and low temperatures; the free energy and the chemical potential in particular turn out to be almost quantitatively predicted [24].

As far as the SCOZA theory is concerned, this represents an advanced liquid state theory that is based on a mean-spherical (MSA) type closure relation, replacing the prefactor  $\beta$  in the closure for the direct correlation function by a yet undetermined, state dependent function  $K(\rho, T)$ ; this function is fixed by the consistency requirement between the energy and the compressibility route to thermodynamics [26, 27]. Thus for a hard-core potential of diameter  $\sigma_{hs}$  and with an attractive tail  $w(r)$ , the SCOZA closure relations to the OZ equation (9) read:

$$g(r) = 0 \quad r < \sigma_{hs} \quad (14)$$

$$c(r) = c_{hs}(r) + K(\rho, T)w(r) \quad r \geq \sigma_{hs}. \quad (15)$$

In relation (15)  $c_{hs}(r)$  represents the direct correlation function for the hard-core system; we have used the Waisman parameterization [48], i.e.,  $c_{hs}(r) = K_0/r \exp[-z_0(r - \sigma_{hs})]$  (with well-described density-dependent coefficients  $K_0$  and  $z_0$ ) which is known to give accurate results for the hard sphere system. The consistency requirement between the two thermodynamic

routes mentioned above leads to the partial differential equation (PDE):

$$\frac{\partial}{\partial \beta} \left( \frac{1}{\chi_{red}} \right) = \rho \frac{\partial^2 u}{\partial \rho^2}, \quad (16)$$

where  $\chi_{red} = \chi_T/\chi_0$  is the reduced (with respect to the ideal gas) dimensionless isothermal compressibility given by the compressibility route and  $u$  is the excess (over ideal gas) internal energy per volume provided by the energy route. Solution of the above PDE leads to  $K(\rho, T)$  and thus to the structure and thermodynamics of the system.

The SCOZA has proven to give reliable results for the location of the coexistence curve and stays — in contrast to most liquid state theories — reliable even in the critical region (see [27] for an overview). Many examples for continuum systems as well as for spin systems (in few cases including even binary mixtures [49]) have demonstrated its validity. Limiting our considerations on continuum systems, the SCOZA suffers from two drawbacks (at least in its present version), despite its many merits: as the formalism of the SCOZA largely benefits from the availability of the semianalytic solution of the MSA for a hard-core Yukawa system (including an arbitrary number of Yukawa tails) [50], its application is limited to systems where the attractive part of the interatomic potential,  $w(r)$ , can be approximated by a suitable number of Yukawa tails, while the repulsive core *has* to be replaced by a hard-core potential. In the present work this has been done at the node of the potential,  $r_0$ , as the SCOZA PDE becomes unstable for repulsive interactions. While in general the first problem does not represent a serious restriction, up to now no remedy has been found to include softness of the repulsive part of the interaction.

### III. RESULTS AND DISCUSSION

In the first part of this section (Figs. 1-3) we compare the perturbation theory for the solid phase with the corresponding Monte Carlo results [11]. Then, the PT free energies are combined with the simulation data for the fluid phase in order to determine the solid-fluid boundaries. In the second part (Figs. 4-6) we present a complementary approach where the MHNC and SCOZA theories are used to predict the liquid-vapor equilibrium, and — in combination with the simulation inputs for the solid phase [11] — the full phase diagram. Hinging on both comparisons, we have calculated in the last part (Fig. 7) the phase diagram on the basis of purely theoretical approaches.

As far as the PT is concerned, the expression (5) gives a hard-core equivalent diameter smoothly varying from  $\sigma_{BH} = 0.970$  nm at  $T = 2200$  K to  $\sigma_{BH} = 0.972$  nm at  $T = 1800$  K. Such a weak variation reflects clearly the stiff, rapidly varying nature of the repulsive part of the Girifalco potential. The more refined expression (4) for

the hard-core diameter,  $\sigma_{\text{WCA}}$ , which adds a further dependence on the density, involves just a minor correction to  $\sigma_{\text{BH}}$  evaluated through Eq. (5).

We report in Figs. 1-2 the PT free energy, chemical potential and equation of state along several isotherms in the solid phase, as obtained by using either  $\sigma_{\text{WCA}}$  or  $\sigma_{\text{BH}}$  as hard-sphere diameter, together with approximations (2) or (6) for the free energy. In the figures, the theoretical predictions are compared to the corresponding simulation results [11]. As can be expected, the use of either  $\sigma_{\text{WCA}}$  or  $\sigma_{\text{BH}}$  produces similar results. The PT predictions generally agree with simulation data all over the solid phase, especially in the chemical potential vs the pressure. The equation of state compares less favorably to Monte Carlo results (see Fig. 2), although wider discrepancies occur for  $\rho \geq 1.27 \text{ nm}^{-3}$ , i.e. almost outside the coexistence region, since the melting line is located between  $\rho \simeq 1.25$  and  $\rho \simeq 1.27 \text{ nm}^{-3}$ . Remarkably, the accuracy of the numerical estimates in the expression (2) results from the balance between two almost comparable — and relatively large with respect to their difference — contributions of opposite signs. The PT predictions slightly get worse if the second order correction to the free energy (however small, since it hardly exceeds 2% of the main contributions) is taken into account. As observed in the original paper [39], this can depend on the semimacroscopic derivation of the last term in Eq. (6), that is more appropriate for longer interaction ranges, in such a way that a reasonably large number of particles fits into the region of attractive potential. The derivative of the pressure involved in Eq. (6) can as well represent a source of numerical uncertainties.

We may anticipate that the fine reproduction of the chemical potential, as obtained through the first-order PT, eventually leads to the most accurate predictions for the phase behavior of the model. For such reason, we concentrate on the expansion (2) and show, in Fig. 3, the corresponding phase diagram; predictions corresponding both to  $\sigma_{\text{WCA}}$  and to  $\sigma_{\text{BH}}$  are reported. The coexistence lines are determined by using the simulation results of Ref. [11] for the fluid phase. It appears that the PT gives accurate predictions for the coexisting temperatures and densities, with marginal effects related to distinct prescriptions for the hard-core diameter. By converse, a systematic overestimate characterizes the coexistence pressure above the triple point (see bottom panel of Fig. 3), especially if  $\sigma_{\text{WCA}}$  is employed. We argue in this latter case that the definition of the cavity function inside the hard core [40], directly borrowed from the theory of simple fluids [46], is to some extent inappropriate for the  $\text{C}_{60}$  model; moreover, numerical uncertainties can occur, due to the more cumbersome procedure needed to evaluate  $\sigma_{\text{WCA}}$  through Eq. (4), which involves in particular the calculation of the slope of  $\bar{g}_{\text{hs}}(r)$  at close contact.

In summary, it turns out that a PT first-order expansion of the model's free energy around a properly defined reference solid gives reliable predictions for the coexistence properties, and, more generally, for the solid phase

behavior of the system at issue. This finding is noteworthy in that it implies that the hard-sphere behavior dominates, to a large extent, the structure of the solid phase; conversely, as discussed in [11], the properties of the fluid phase are markedly affected by energetic aspects related to the attractive part of the potential. Our results further support the use of the PT to characterize the solid phase of systems interacting through short-range forces, already documented in Refs. [31, 32, 33].

As far as the theoretical description of the fluid phase is concerned, we report in Fig. 4 the SCOZA and MHNC predictions for the free energy, the chemical potential, the pressure, and the internal energy, along with the corresponding Monte Carlo results of Ref. [11]. It appears that the MHNC predicts to a high accuracy the chemical potential as a function of the pressure, a quantity directly related to the coexistence properties of the model. A satisfactory agreement with the simulation data also emerges for both the free and the internal energies, while a marked discrepancy affects the estimate of the pressure, especially in the high-density regime. On the other hand, as is visible in Fig. 4, the thermodynamic properties of the model are generally overestimated in the SCOZA framework.

The tendency of the MHNC to overestimate the pressure under the global consistency procedure, already observed in Ref. [24], appears somehow unexpected, especially considering the overall good performances of this theory. We can conjecture that it might depend on an overestimate of the effective hard-sphere diameter  $\sigma_{\text{hs}}^*$  entering the bridge function as the adjustable parameter to enforce the thermodynamic consistency in Eq. (11) or (12). Indeed, the value of the virial pressure  $P_v$  depends on a delicate balance between contributions of opposite signs. The use of the Verlet-Weis bridge functions (which fit available simulation data), instead of the analytical Percus-Yevick ones, might as well improve the predictions for the pressure. As for the SCOZA, we argue that the discrepancies with simulation data must be related to the approximate treatment of the repulsive part of the potential. In particular, the substitution of the soft-core interaction with a purely hard-sphere potential for  $r < r_0$  causes an enhanced repulsion (which reflects in the overestimate of the free energy and of the pressure), especially at high temperature, where shorter distances can be sampled by the system. We have indeed verified by few simulation runs along the isotherm  $T = 2100 \text{ K}$  (not reported here) that the agreement between SCOZA and Monte Carlo pressures considerably improves, provided that both approaches are compared on the same model, i.e. hard-spheres plus a Girifalco tail.

We report in Fig. 5 the SCOZA and MHNC predictions for the liquid-vapor coexistence properties of the model. The Gibbs Ensemble Monte Carlo (GEMC) binodal line obtained in Ref. [15] with a sample of 1500 particles is also shown for comparison. It comes out that both theories reproduce quite faithfully the binodal curve, especially as far as the vapor branch is concerned. The co-

TABLE I: MHNC and SCOZA critical and triple point densities (in  $\text{nm}^{-3}$ ) and temperatures (in K). Simulations: the critical point corresponds to the GEMC estimate with 1500 particles of Ref. [15]; the triple point has been calculated in Ref. [11].

	MHNC	SCOZA	Simulations
$T_{\text{cr}}$	1929	1957	1940
$\rho_{\text{cr}}$	0.408	0.432	0.43
$T_{\text{tr}}$	1867	1916	1880
$\rho_{\text{tr}}$	0.70	0.64	0.73

existing liquid densities are slightly underestimated, the SCOZA reverting this trend just below the critical point. The binodal curve obtained through the MHNC under the global consistency constraint definitely improves on the local one, as displayed in Fig. 5, thus confirming the preliminary evidence reported in Ref. [24]. As for the SCOZA, an internal compensation between the overestimate of the chemical potential on one hand, and of the pressure on the other hand, could be at the origin of the fairly good agreement with the GEMC binodal curve.

The MHNC solution algorithm converges to a thermodynamic consistent solution up to  $T = 1900$  K (see Fig. 5). In view of early studies on HNC-type theories (see e.g. [47]), the difficulties to explore the critical region may be intrinsic to such approaches, rather than an artifact of numerical procedures. Consequently, the available MHNC binodal points must be fitted to some expected behavior in order to determine the critical parameters; as a common practice, we have used the scaling law for the coexisting densities to calculate the critical temperature,  $T_{\text{cr}}$ :

$$\rho_{\text{liquid}} - \rho_{\text{vapor}} \propto |T - T_{\text{cr}}|^{\beta}, \quad (17)$$

where the exponent takes on the non-classical effective value  $\beta = 0.32$ . Once the critical temperature is known, we have calculated the critical density,  $\rho_{\text{cr}}$ , by fitting the MHNC binodal points with the law of rectilinear diameter:  $\rho_{\text{liquid}} - \rho_{\text{vapor}} = \rho_{\text{cr}} + A|T - T_{\text{cr}}|$ , with  $A$  to be determined from the fit. At variance with the MHNC, within the SCOZA the critical region can be approached in principle with arbitrary precision and therefore neither a fitting procedure, nor a scaling behavior hypothesis must be invoked to calculate the critical point parameters. It emerges from Fig. 5 that the theoretical predictions closely bracket the GEMC critical point. The MHNC, SCOZA, and GEMC critical parameters are collected in Table I.

In Fig. 6 we report the fluid-solid phase boundaries, as obtained by the combination of the MHNC and SCOZA predictions for the fluid phase and the simulation results of Ref. [11] for the solid phase; for a more comprehensive overview, we also show a sketch of the binodal curves just discussed, as well as the full simulated fluid-solid coexistence points. As it is apparent, the overall good quality of

the MHNC thermodynamic predictions provides a faithful reproduction of the phase boundaries of the model. A small overestimate of the fluid-solid coexistence pressure only occurs above the triple point temperature. As for the SCOZA, the solid-vapor equilibrium and the melting line are satisfactorily predicted, while the observed shift of the chemical potential (see Fig. 4) gives rise to a marked discrepancy in the coexistence pressure above the triple point; on the other hand, the overestimate of the pressure of the fluid phase is reflected in the shift of the theoretical freezing line toward lower densities.

We have determined the MHNC and SCOZA triple points, also reported in Table I, from the intersection between the corresponding binodal and freezing lines. It comes out that the MHNC predicts the existence of a stable liquid phase with a small shift of the triple and critical densities to lower values, with respect to the simulation results. The SCOZA also predicts a liquid pocket for the model, although restricted to a narrower temperature and density range.

It emerges that the MHNC theory for the fluid phase, and the first-order PT for the solid phase represent, among these envisaged here, the most accurate theoretical tools to enquire into the full phase portrait of the  $\text{C}_{60}$  model. The ensuing phase diagram is reported in Fig. 7. The MHNC binodal line is directly drawn from Fig. 5. As is visible, the agreement with simulation data is semiquantitative; the comparison of Figs. 3, 6, and 7 demonstrates that the errors in the location of phase boundaries are essentially brought about by the MHNC, while the use of the PT for the solid phase does not introduce any appreciable discrepancy with simulation results. For such reason we do not expect a significant improvement of the overall appearance of the phase diagram if the SCOZA predictions for the fluid phase substitute the MHNC ones. In the bottom panel of Fig. 7, the overestimate of the fluid-solid coexistence pressure magnifies slightly the common trend already observed for the PT and MHNC approaches separately.

#### IV. SUMMARY AND CONCLUDING REMARKS

We have presented a theoretical investigation of the thermodynamic properties and the phase behavior of the Girifalco  $\text{C}_{60}$  model, in the framework provided by three refined theoretical tools, as the Modified Hypernetted Chain (MHNC) with a global thermodynamic consistency constraint and the Self-Consistent Ornstein-Zernike Approximation (SCOZA) for the fluid phase, and a Perturbation Theory (PT) with various degrees of refinement for the free energy of the solid phase.

The theoretical predictions are assessed against our recent simulation study [11]. It turns out that the phase portrait of the model is predicted fairly well, in particular as for the solid-vapor coexistence and the melting line. By converse, the inaccuracies in the thermodynamic pre-

dictions sensitively affect the determination of the fluid-solid coexistence pressure above the triple point. The MHNC and SCOZA liquid-vapor binodals are sufficiently accurate; the critical point estimates closely bracket the Gibbs Ensemble Monte Carlo datum [15]. In comparison with the simulation and the MHNC freezing lines (which turn to be practically superimposed), the SCOZA tends to underestimate the density of the liquid branch of the fluid-solid coexistence, with a corresponding shift of the triple point to lower densities and higher temperatures.

We have interpreted our results in view of the basic assumptions underlying each theory. It has emerged that the SCOZA mainly suffers from the substitution of the Girifalco soft-core repulsion at short distance with a purely hard-sphere interaction, which leads to a corresponding overestimate of the pressure and of the free energy in the fluid phase. We have also conjectured that the MHNC pressure might improve if the Verlet-Weis bridge functions were adopted instead of the Percus-Yevick ones, as currently adopted in this work. As for the PT, it turns out that both a second order expansion of the free energy, and a refined definition of the equivalent hard-core diameter, lead to a slight worsening of the theoretical predictions on the whole, which could be related to more cumbersome numerical procedures involved.

We have eventually succeeded in predicting to a satisfactory degree of accuracy the phase diagram of the Girifalco model, on the basis of purely theoretical approaches. We have selected for this purpose a sophisticated MHNC treatment of the fluid phase, and the first-order PT for the solid phase. We expect that our conclusions about the most suitable theoretical schemes to investigate the phase diagram of the Girifalco model, can be reasonably extended to other systems characterized by similar interparticle interaction laws. In particular, we plan to analyze the phase diagram of other higher-order  $C_{n>60}$  fullerenes, combining both simulations and theoretical schemes. We have already produced several Monte Carlo results for the Girifalco  $C_{84}$  fullerene, to be used for such purpose. The related calculations are currently in progress.

### Acknowledgments

ESP and GK acknowledge the financial support by the Österreichische Forschungsfonds (FWF) under Project Nos. P14371-TPH and P15758-TPH.

- 
- [1] L. A. Girifalco, J. Phys. Chem. **95**, 5370 (1991); **96**, 858 (1992).
  - [2] J. M. Pacheco and J. P. Prates-Ramalho, Phys. Rev. Lett. **79**, 3873 (1997); A. L. C. Ferreira, J. M. Pacheco, and J. P. Prates-Ramalho J. Chem. Phys. **113**, 738 (2000).
  - [3] R. P. S. Fartaria, F. M. S. Silva Fernandes, and F. F. M. Freitas, J. Phys. Chem. B **106**, 10227 (2002).
  - [4] M. C. Abramo, C. Caccamo, D. Costa, and G. Pellicane, Europhys. Lett. **54**, 468 (2001).
  - [5] F. Micali, M. C. Abramo and C. Caccamo, J. Phys. Chem. Solids **64**, 319 (2003).
  - [6] F. M. S. Silva Fernandes, F. F. M. Freitas, and R. P. S. Fartaria, J. Phys. Chem. B **107**, 276 (2003).
  - [7] E. Schöll-Paschinger and G. Kahl *submitted for publication to Europhysics Lett.* (2003).
  - [8] U. S. Schwarz and S. A. Safran, Phys. Rev. E **62**, 6957 (2000).
  - [9] O. Umiguchi, T. Inaoka, and M. Hasegawa, J. Phys. Soc. Japan **68**, 508 (1999).
  - [10] M. Hasegawa and K. Ohno, J. Chem. Phys. **111**, 5955 (1999).
  - [11] D. Costa, G. Pellicane, C. Caccamo, and M. C. Abramo, J. Chem. Phys. **118**, 304 (2003).
  - [12] M. H. J. Hagen, E. J. Meijer, G. C. A. M. Mooij, D. Frenkel, and H. N. W. Lekkerkerker, Nature **365**, 425 (1993).
  - [13] A. Cheng, M. L. Klein, and C. Caccamo, Phys. Rev. Lett. **71**, 1200 (1993).
  - [14] M. Hasegawa and K. Ohno, J. Phys.: Cond. Matter **9**, 3361 (1997).
  - [15] C. Caccamo, D. Costa, and A. Fucile, J. Chem. Phys. **106**, 255 (1997).
  - [16] C. Caccamo, Phys. Rev. B **51**, 3387 (1995).
  - [17] F. M. S. Silva Fernandes, R. P. S. Fartaria, and F. F. M. Freitas, Comp. Phys. Comm. **141**, 403 (2001).
  - [18] D. Costa, C. Caccamo, and M. C. Abramo, J. Phys.: Cond. Matter **14**, 2181 (2002).
  - [19] A. A. Louis, Philos. Trans. R. Soc. London Ser. A **359**, 939 (2001).
  - [20] L. Mederos and G. Navascués, Phys. Rev. B **50** 1301 (1994).
  - [21] M. Hasegawa and K. Ohno, Phys. Rev. E **54**, 3928 (1996).
  - [22] M. Tau, A. Parola, D. Pini, and L. Reatto, Phys. Rev. E **52**, 2644 (1995).
  - [23] Y. Rosenfeld and N. W. Ashcroft, Phys. Rev. A **20**, 1208 (1979).
  - [24] C. Caccamo and G. Pellicane, J. Chem. Phys. **117**, 5072 (2002).
  - [25] J. S. Høye and G. Stell, J. Chem. Phys. **67**, 439 (1977).
  - [26] D. Pini, G. Stell, and N.B. Wilding, Mol. Phys. **95**, 483 (1998).
  - [27] E. Schöll-Paschinger, PhD thesis (Technische Universität Wien, 2002; unpublished); thesis available from the homepage: <http://tph.tuwien.ac.at/~paschinger/> and download 'PhD'.
  - [28] G. Kahl, E. Schöll-Paschinger, and G. Stell, J. Phys.: Cond. Matter **14**, 9153 (2002).
  - [29] J.-P. Hansen and L. Verlet, Phys. Rev. **184**, 151 (1969).
  - [30] P. V. Giaquinta and G. Giunta, Physica A **187**, 145 (1992); F. Saija, S. Prestipino and P. V. Giaquinta, J. Chem. Phys. **115**, 7586 (2001), and references therein.
  - [31] Ph. Germain and S. Amokrane, Phys. Rev. E **65**, 031109

- (2002).
- [32] E. Velasco, G. Navascués, and L. Mederos, Phys. Rev. E **60**, 3158 (1999).
  - [33] G. Foffi, G. D. McCullagh, A. Lawlor, E. Zaccarelli, K. A. Dawson, F. Sciortino, P. Tartaglia, D. Pini, and G. Stell, Phys. Rev. E **65**, 031407 (2002).
  - [34] J. P. Hansen and I. R. McDonald, *Theory of Simple Liquids* 2nd ed. (Academic Press, New York, 1986).
  - [35] J. J. Weis, Molec. Phys. **28**, 187; Molec. Phys. **32**, 296 (1976).
  - [36] C. Rascon, L. Mederos and G. Navascues, Phys. Rev. E **54**, 1261 (1996); Phys. Rev. Lett. **77**, 2249 (1996).
  - [37] J. D. Weeks, D. Chandler, and H. C. Andersen, J. Chem. Phys. **54**, 5237 (1971).
  - [38] H. C. Andersen, J. D. Weeks, and D. Chandler, Phys. Rev. A **4**, 1597 (1971).
  - [39] J. A. Barker and D. Henderson, J. Chem. Phys. **47**, 4714 (1967).
  - [40] Y. Choi, T. Ree, and F. H. Ree, J. Chem. Phys. **95**, 7548 (1991).
  - [41] J. A. Barker and D. Henderson, J. Chem. Phys. **47**, 2856 (1967).
  - [42] K. R. Hall, J. Chem. Phys. **57**, 2252 (1972).
  - [43] B. Alder, W. G. Hoover, and D. A. Young J. Chem. Phys. **49**, 3688 (1968).
  - [44] D. Frenkel and A. J. C. Ladd, J. Chem. Phys. **81**, 3188 (1984).
  - [45] J. M. Kincaid and J. J. Weis, Molec. Phys. **34**, 931 (1977).
  - [46] D. Henderson and E. W. Grundke, J. Chem. Phys. **63**, 601 (1975).
  - [47] C. Caccamo, Phys. Rep. **274**, 1 (1996).
  - [48] E. Waisman, Mol. Phys. **25**, 45 (1973).
  - [49] E. Schöll-Paschinger and G. Kahl, J. Chem. Phys. (in press).
  - [50] E. Arrieta, C. Jędrzejek, and K.N. Marsh, J. Chem. Phys. **95**, 6806 (1991).



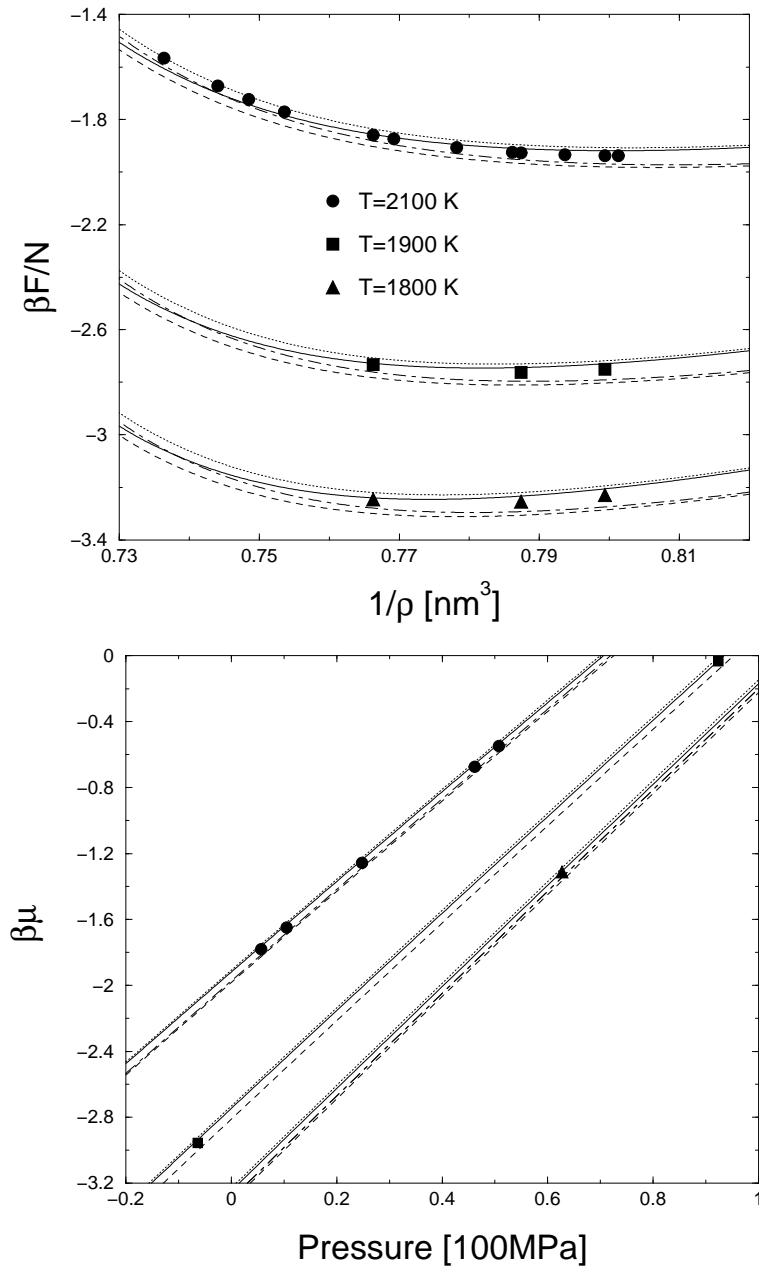


FIG. 1: PT free energy (top) and chemical potential (bottom) along three isotherms in the solid phase: first-order PT (Eq. (2)) with  $\sigma_{\text{WCA}}$  (Eq. (4), dotted line) or  $\sigma_{\text{BH}}$  (Eq. (5), full line), as equivalent hard-core diameters; second order PT (Eq. (6)) with  $\sigma_{\text{WCA}}$  (dot-dashed line) or  $\sigma_{\text{BH}}$  (dashed line). Symbols represent the corresponding Monte Carlo results [11].

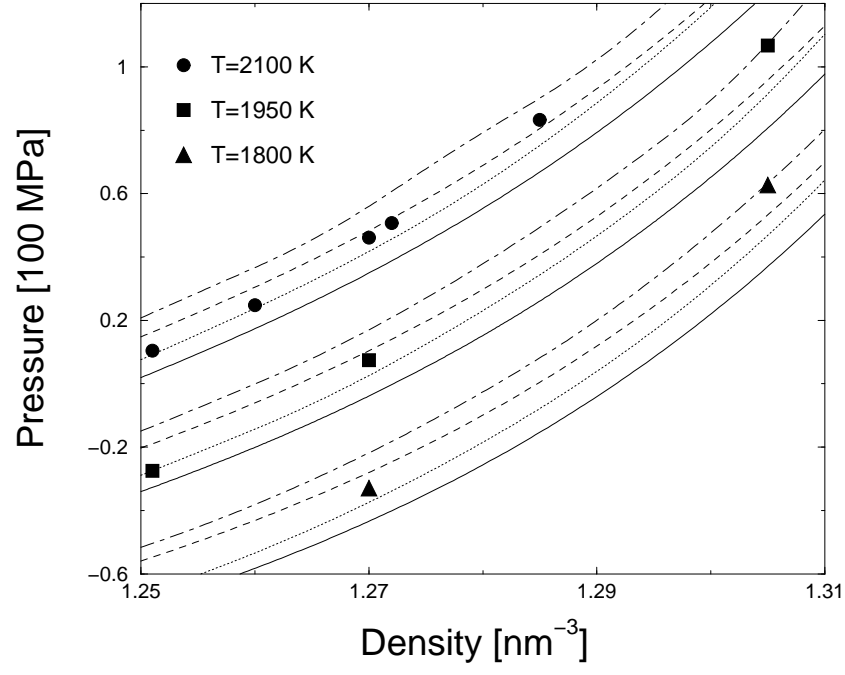


FIG. 2: PT equation of state in the solid phase (lines), displayed in order of decreasing temperature from top to bottom, according to the legend of Fig. 1. Symbols: corresponding Monte Carlo results [11]. For clarity sake the isotherms  $T = 2100$ ,  $1950$ , and  $1800$  K are displayed.

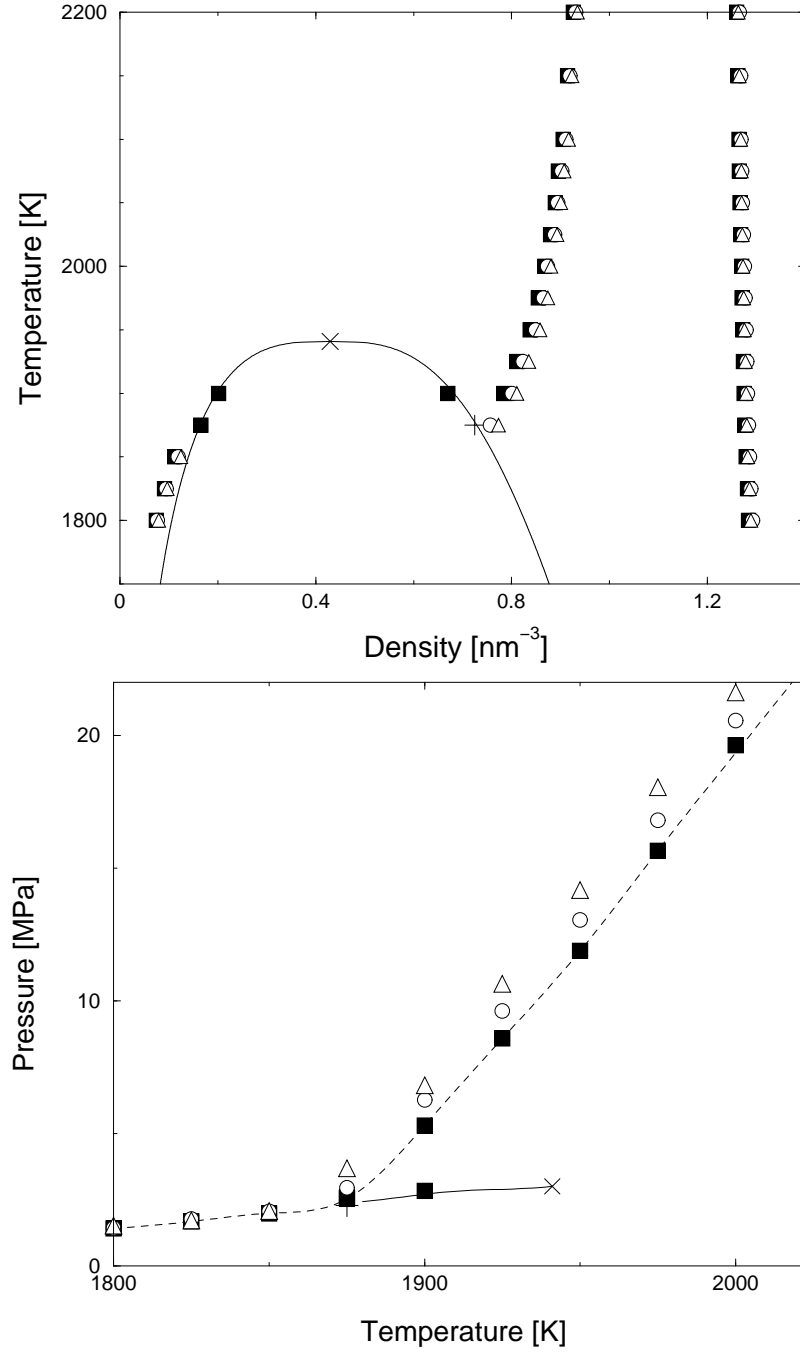


FIG. 3: First-order PT fluid-solid coexistence densities (top) and pressures (bottom) of the  $C_{60}$  model, with  $\sigma_{\text{WCA}}$  (triangles) or  $\sigma_{\text{BH}}$  (circles) as hard-core diameters. Squares: Monte Carlo results [11]. For completeness, the GEMC liquid-vapor coexistence densities (top) and pressures (bottom) are also shown as full lines [15]. The cross and the plus indicate the simulation critical and triple points, respectively. In the bottom panel dashed lines are guides to the eye for the Monte Carlo results.

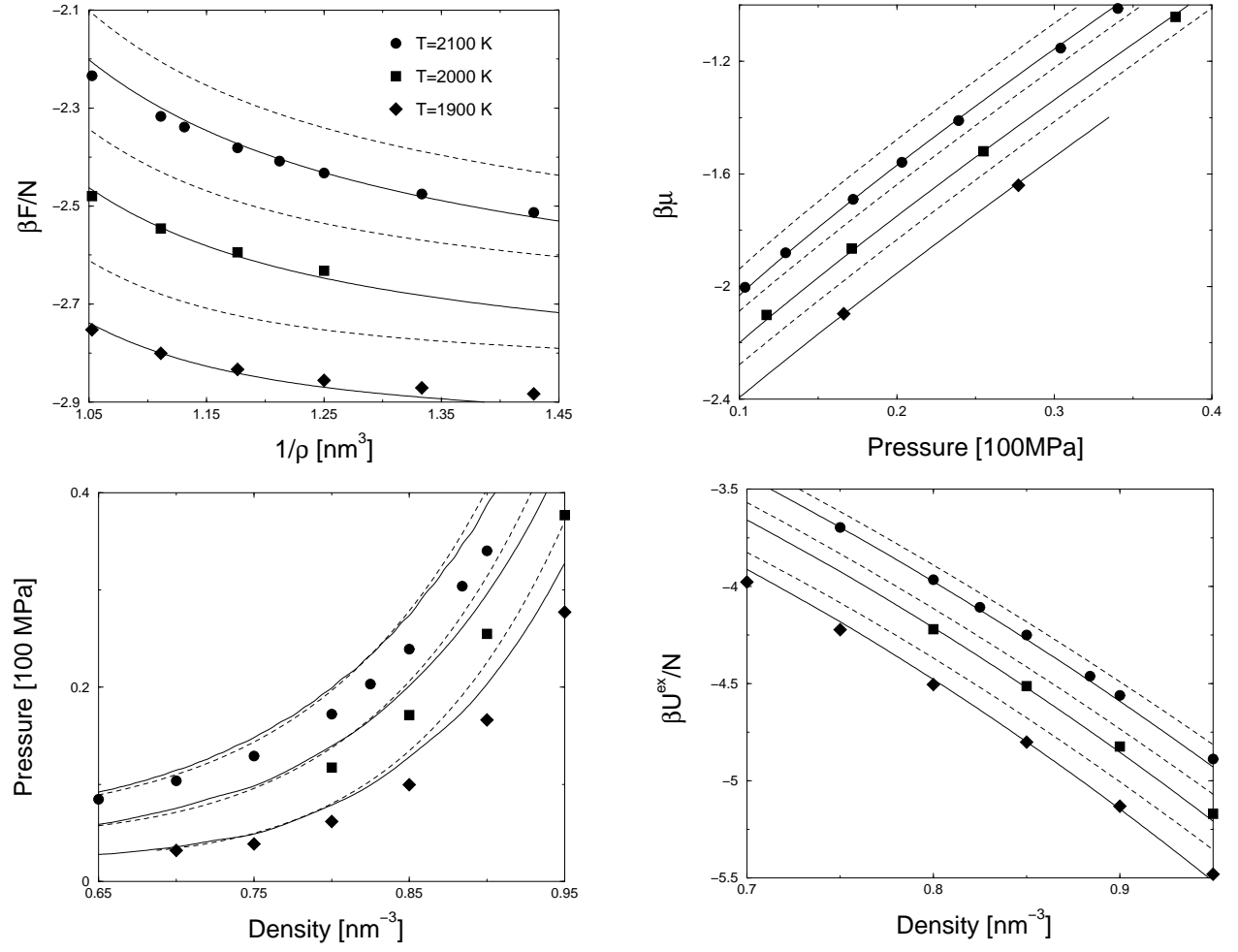


FIG. 4: MHNC (full lines) and SCOZA (dashed lines) thermodynamic properties along three isotherms in the fluid phase. Symbols: Monte Carlo results [11] at  $T = 2100$  K (circles),  $2000$  K (squares) and  $1900$  K (diamonds). All curves are displayed from top to bottom in order of decreasing temperature.

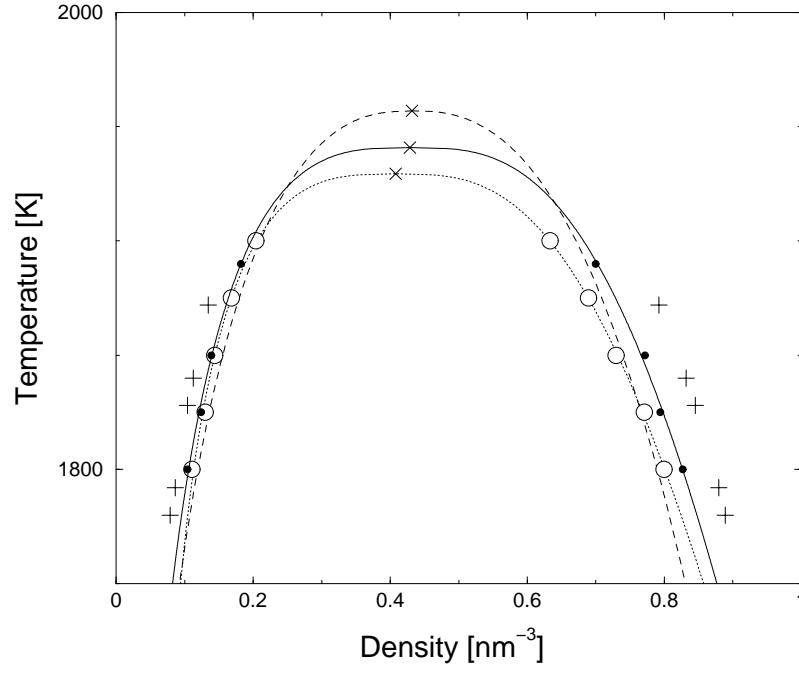


FIG. 5: MHNC (dotted line with open circles) and SCOZA (dashed line) liquid-vapor coexistence; the GEMC results (full line with dots, [15]) are also shown. The crosses are the critical points. Pluses: MHNC under a local consistency constraint [16]. The calculated coexistence points are shown as open circles (MHNC) and dots (GEMC) while the lines represent corresponding theoretical interpolations.

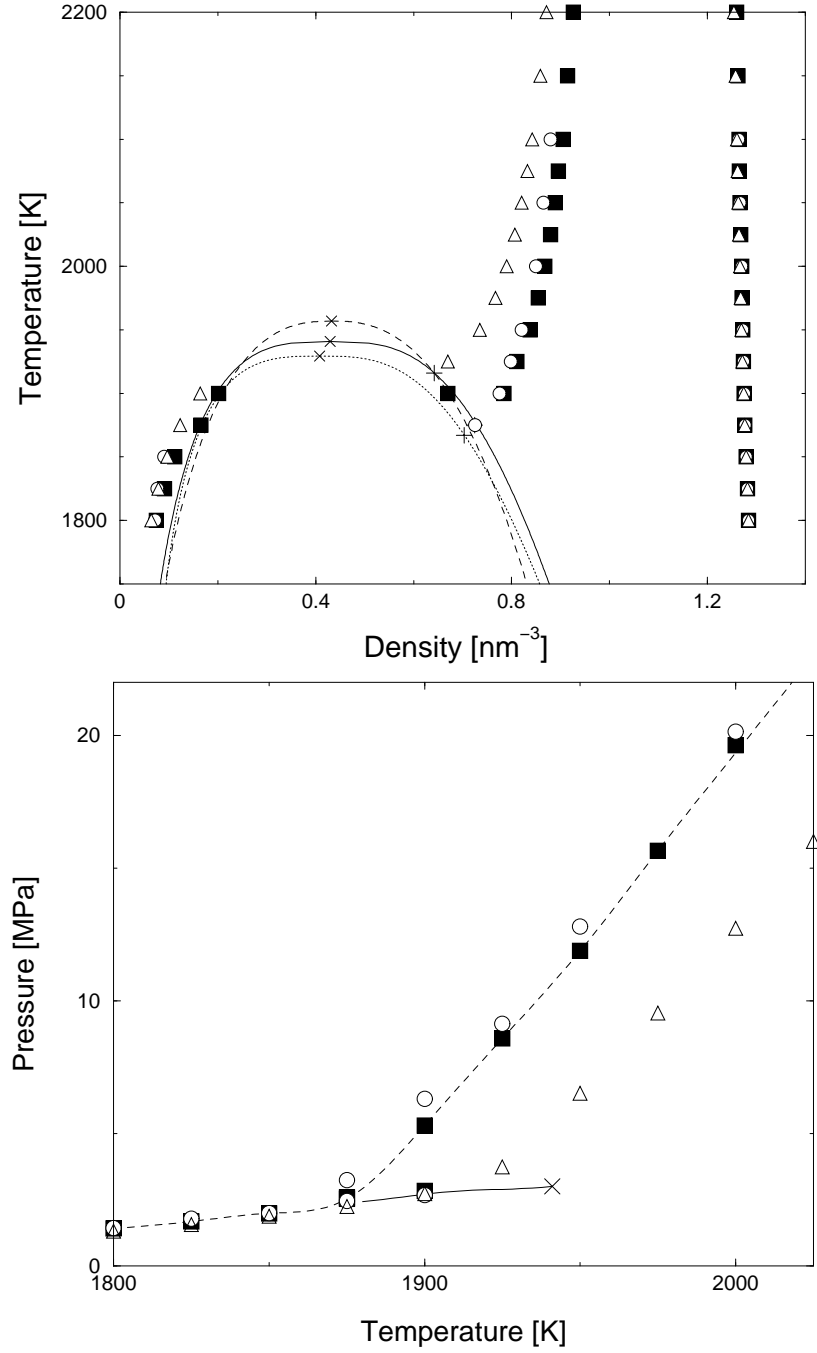


FIG. 6: MHNC (circles) and SCOZA (triangles) fluid-solid coexistence densities (top) and pressures (bottom). Squares: Monte Carlo results [11] with the corresponding triple point (plus). For completeness, the binodal curves drawn in Fig. 5 are also reported in the top panel. In the bottom panel the full line is the GEMC liquid-vapor coexistence pressure [15] with the corresponding critical point (cross); dashed lines are guides to the eye for the simulation results.

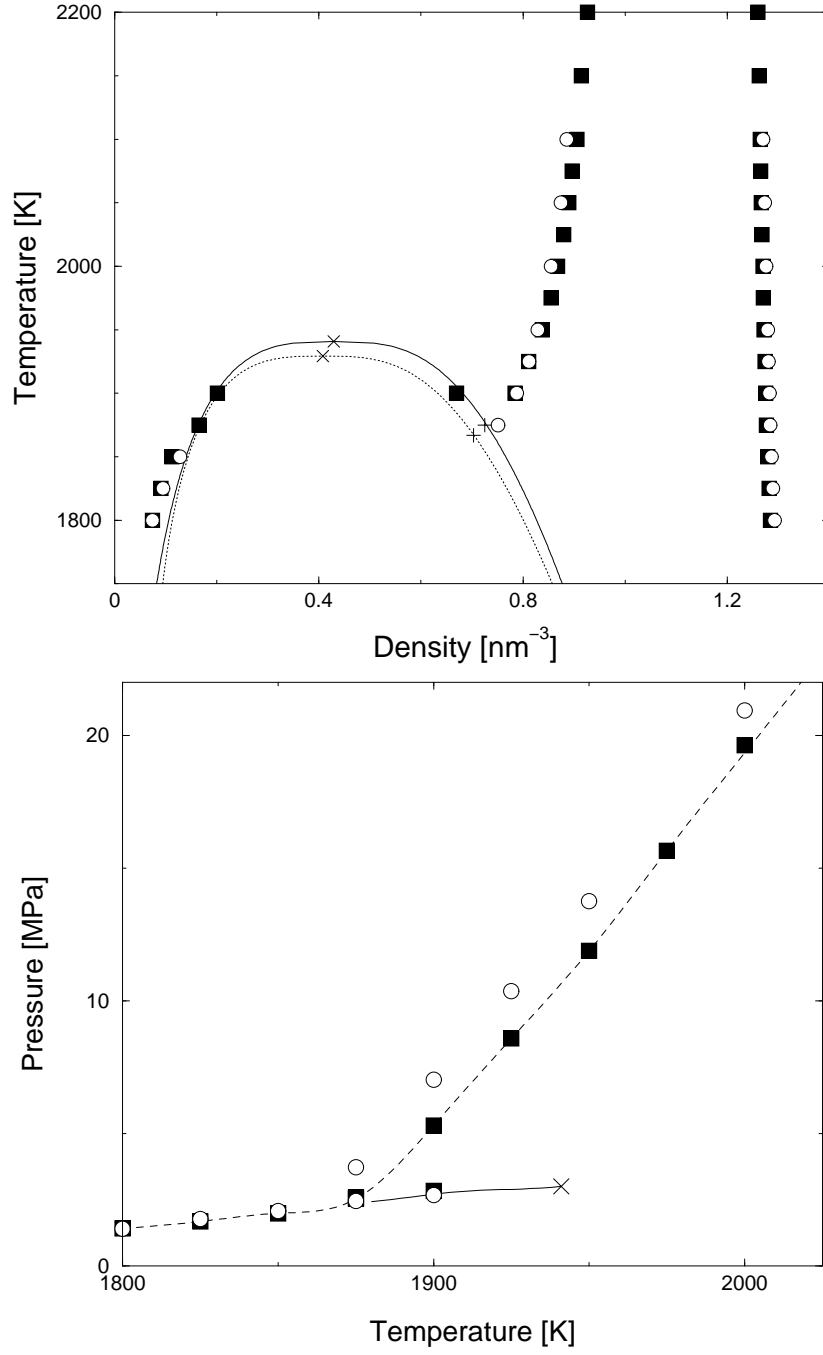


FIG. 7: Circles: fully theoretical fluid-solid coexistence densities (top) and pressures (bottom) of the  $C_{60}$  model. Squares: simulation results [11]. The MHNC and GEMC binodal curves with corresponding critical points shown in Fig. 5 are also displayed. In the bottom panel the full line is the GEMC liquid-vapor coexistence pressure [15] with the corresponding critical point (cross); dashed lines are guides to the eye for the simulation results.